On the manipulability of swing foot and stability of human locomotion

Miripour Fard, Behnam; Bruijn, Sjoerd M.

published in
Multibody System Dynamics
2019

DOI (link to publisher)
10.1007/s11044-018-09664-y

document version
Publisher's PDF, also known as Version of record

Multibody Syst Dyn
https://doi.org/10.1007/s11044-018-09664-y

On the manipulability of swing foot and stability of human locomotion

Behnam Miripour Fard[1] · **Sjoerd M Bruijn**[2]

Received: 16 June 2018 / Accepted: 15 December 2018

Abstract Manipulability is a measure that quantifies the range of possible motions of a robotic end-effector and it is also an important measure in the study of coordination of human upper body and grasping tasks. This measure, which is defined on both the kinematic and dynamic level, could be useful in gait, as it could be used to determine potential foot placement possibilities. Kinematic manipulability is defined based on the Jacobian and dynamic manipulability on both the Jacobian and mass-inertia matrix. The main purpose of this study was to evaluate the manipulability of human walking and to explore a possible relation between the manipulability and dynamic stability of walking at different speeds. A 37-DoF tree-like model of the human body was developed to evaluate the manipulability index of human walking. We measured kinematics of 11 healthy male subjects while walking on a treadmill, and mapped the data to the model using inverse kinematics. Jacobian based kinematic/dynamic manipulability measures of walking were evaluated for the swing phase of walking. Manipulability ellipsoids were drawn for geometric determination of this measure in all directions during early, mid- and late swing phases. As stability metrics, the local divergence exponent and Floquet Multipliers were calculated. The results indicated a high kinematic manipulability of the swing foot during early and late swing phases and a drop in kinematic manipulability during mid-swing. Kinematic manipulability of the swing leg during early and late (but not mid-) swing phases increased with walking speed but the average kinematic manipulability of the center of mass and dynamic manipulability of swing foot decreased with increasing walking speed. Moreover, the results showed a weak relation between the manipulability and local and orbital stability.

Keywords Bipedal walking · Manipulability · Stability · Optimization

✉ B. Miripour Fard
bmf@guilan.ac.ir

[1] Faculty of Mechanical Engineering, University of Guilan, Rasht, Guilan 41938-33697, Iran

[2] Department of Human Movement Science, VU university, Amsterdam, Netherlands

Published online: 11 January 2019

1 Introduction

In the field of robotics, manipulability analysis is an effective tool for evaluation of the ability of a manipulator for performing velocities and accelerations at the end-effector in all directions. When a manipulability measure reaches zero, the manipulator is in a singular pose, and it cannot move in some directions. Manipulability is quantified using the Jacobian of the manipulator. Given an end effector position, the manipulability measure is usually used to find an optimal configuration or an optimal set of link lengths to make the manipulator as dexterous as possible [16]. This works especially well in the case of redundant manipulators because they can satisfy additional desirable task(s).

Several studies have investigated manipulability and dexterity for the design and control of redundant manipulators [5, 9, 21, 23, 24, 38, 42]. Bipedal robots, and the human body, can be modeled as a set of serial redundant manipulators such as legs, arms, and head, all connected together at the trunk. The end of each of these manipulators can be considered as an end effector. So, analysis performed on the manipulability of manipulators can be extended to bipeds (either robots or humans). However, in the case of bipedal walking, there is a lack of comprehensive studies on manipulability. For example, the profile of manipulability of the swing foot over the gait cycle has not been studied. The kinematic manipulability of the swing foot indicates the set of velocities that can be achieved by the tip of the swing foot. Manipulability can directly influence possible step directions and foot placement possibilities, and consequently may be of great interest in the study of stability and maneuverability of walking [1, 36].

Previous studies on the manipulability of bipeds can be classified into two categories: (i) those studying manipulability and coordination of upper degrees of freedom (DoFs) for hand movements and grasping tasks [7, 14, 15, 18, 19, 37], and (ii) those studying manipulability and dexterity analysis of walking and whole body movements. There are also some studies addressing both of the above-mentioned categories.

Exploring the first category is beyond the scope of the current work, and we will briefly review studies on the manipulability analysis of biped walking. Inoue et al. [13] proposed a controller not only based on stability but also on manipulability for a humanoid robot doing tasks with the hands while walking. The effectiveness of the method was shown by computer simulations and experiments on a small humanoid robot. Maneewarn and Boonprakob [20] modified the trajectory of a biped robot off-line using the kinematic manipulability information about the swing foot to reduce energy consumption and increase walking stability. The method was tested on a small-size humanoid robot and the results were promising. Ota et al. [26] considered the loss of manipulability due to reduction of DoF in development of an 8-DoF biped robot. Xiao et al. [41] investigated the pushing manipulation by humanoid robot BHR-2 during dynamic walking. In this research, dual arm kinematic manipulability was analyzed by using the known leg trajectory and hands posture. Samy and Kheddar [32] addressed the problem of safe falls for humanoid robots and proposed a new controller based on the manipulability. Tagawa and Yamashita [35] applied the concept of manipulability to measure the controllability of motion of the body in robotic bipedal locomotion. It was suggested that in studying the kinematics and dynamics of bipeds, locomotion and manipulation should be considered without separation because similarities seem to exist between these functions. Some studies have used the concept of manipulability in a dynamic level [2, 17, 22, 33]. Center of mass (CoM) manipulability and zero moment point (ZMP) manipulability have also been studied in previous studies. Naksuk and Lee [25] introduced the ZMP Manipulability Ellipsoid as an extension to the existing ZMP balance criterion. The shape and size of the ellipsoid of this measure represent the degree of the ability of

a humanoid robot to instantly move the ZMP. They have formulated the manipulability of the ZMP based on the manipulability of the CoM and showed that this measure can aid the design process of humanoid robots. Cotton et al. [6] used the center of mass (CoM) kinematic manipulability and dynamic manipulability for humanoid robot design optimization to characterize the capacity to generate any spatial acceleration of the CoM. They concluded that the CoM dynamic manipulability is a valuable index in the field of humanoid robotics. Gu et al. [10] suggested that gait stability of a humanoid robot is closely related to the Feasible Center of Mass Dynamic Manipulability (FCDM). This index indicates the ability of a humanoid robot to regulate its CoM motion at a given posture under ground-contact constraints. Padois et al. [27] addressed using the kinematic manipulability of the CoM as a metric to measure the effects of the environmental contacts on the legged robot's stability. The kinematic manipulability of the CoM relates the actuated joint velocities of the robot to the linear velocity of the CoM. They showed that instantaneous change of the CoM velocity, due to the unit norm impulse at the joints, for the constrained robot is always higher than that of the unconstrained robot.

In all of the above-mentioned studies, the manipulability was not investigated by looking at the real human behavior. Given the recent interest in foot placement based stability analysis [30, 39], it seems that an experimental analysis of manipulability of human walking could be of great interest for those studying human and humanoids gait stability. However, as discussed above, little is still known about the following: (a) variation of the manipulability of the swing limbs of human during walking, (b) the effect walking speed on the manipulability of swing foot, (c) variation of the manipulability of CoM and its correlation with stability, and (d) relation between the manipulability and local and orbital stability of walking. The main purpose of the current study is to address these issues with the aim of gaining more insight into the manipulability of walking for future use in robotics and biomechanics.

2 Model and experimental method

2.1 Multibody modeling and kinematics

The human body was modeled using a series of rigid links connected by revolute joints. The model of the current study is presented in Fig. 1. With consideration of 6 global DoFs, the total number of DoFs of the model is 37. The model has a tree-like structure. Each of the 14 segments of the model can be considered as the base or the root. In the current study, the stance foot is chosen as the root. Considering one of the feet as the support, there are three branches for the model: the swing leg, right arm and left arm. It is obvious that in this tree-structured kinematic chain, some joints do not influence the motion of some chains. The model consists of three serial substructures. For each of the serial substructures, the serial segment conventions are used without change. The Denavit–Hartenberg (DH) notation is used for geometric description of the model. Based on [34], the forward kinematics of the model are derived using DH tables and transformation matrix (see Appendix A).

The Jacobian is calculated only for the swing phase of walking. The model has three serial substructures with three end-effectors. So, the body velocity in the right hand of (1) is a $6N \times 1$ vector ($N = 3$), and the Jacobian matrix is a $6N \times 31$ matrix ($N = 3$)

$$\begin{bmatrix} \xi_1 \\ \xi_2 \\ \xi_3 \end{bmatrix} = \begin{bmatrix} J_1^1 & J_1^2 & J_1^3 \\ J_2^1 & J_2^2 & J_2^3 \\ J_3^1 & J_3^2 & J_3^3 \end{bmatrix} \begin{bmatrix} \dot{q}_1 \\ \vdots \\ \dot{q}_{31} \end{bmatrix}, \tag{1}$$

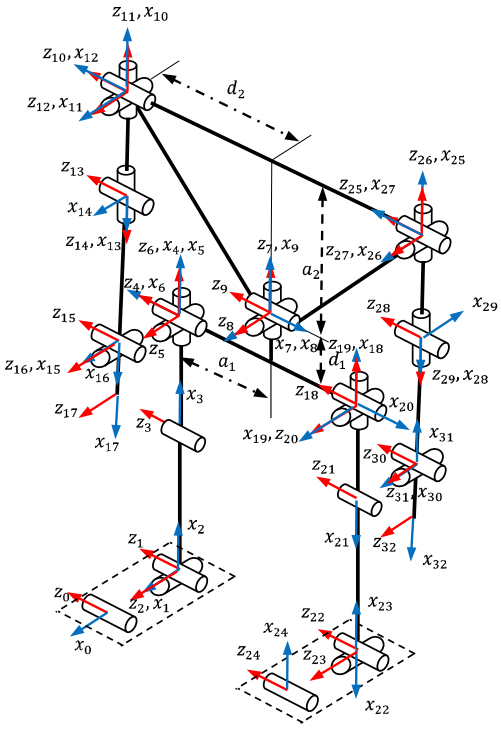

Fig. 1 Model of this study and DH coordinate frame assignment: $x_i\, z_i$ represent the DH coordinates (Appendix A), a_i and d_i are the constant anthropometric parameters

in which ξ_i $(i = 1, \ldots, 3)$ is a 6×1 vector containing the linear and angular velocities of the end-effector i; q_i is the joint angle and J_i^j is a $6 \times m$ matrix where the m depends on the number of the joints that influence the velocity of the corresponding end-effector. There are 9 different values of m. Formally, (1) can be expressed as

$$\xi = \mathbf{J}(\mathbf{q})\dot{\mathbf{q}}. \tag{2}$$

The Jacobian matrix has many zero elements at the places where some joints do not influence the motion of some end-effectors.

2.2 Manipulability

The kinematic manipulability [42] is defined based on the Jacobian of the robot as

$$w_k = \sqrt{\det\left[\mathbf{J}(\mathbf{q})\mathbf{J}(\mathbf{q})^{\mathrm{T}}\right]} = s_1 s_2 \cdots s_n, \tag{3}$$

in which s_i is the singular value of the Jacobian ($\mathbf{J}(\mathbf{q})$), det is the determinant, and n is the number of DoFs. Higher values of w imply that the manipulator is in a posture that gives it a better ability to move. For a given configuration of a manipulator, the ellipsoid of kinematic manipulability is drawn considering unit norm joint velocities as input ($\|\dot{\mathbf{q}}\| = 1$). The equation of the kinematic manipulability ellipsoid is given by

$$\boldsymbol{\xi}^{\mathrm{T}}\left(\mathbf{J}(\mathbf{q})\mathbf{J}(\mathbf{q})^{\mathrm{T}}\right)^{-1}\boldsymbol{\xi} \leq 1. \tag{4}$$

The size and shape of the kinematic manipulability ellipsoid are important for kinematic analysis. For a given configuration, the longest principal axis of the ellipsoid shows the direction and the amplitude of the maximum velocity that can be reached by the end effector.

Dynamic manipulability measure has been defined in [38] which takes into consideration the dynamics of motion. The dynamics equation of manipulators is generally presented as follows:

$$\mathbf{M}(\mathbf{q})\ddot{\mathbf{q}} + \mathbf{C}(\mathbf{q}, \mathbf{q})\dot{\mathbf{q}} + \mathbf{G}(\mathbf{q}) = \tau, \tag{5}$$

where $\mathbf{M}(\mathbf{q}) \in \mathbb{R}^{31\times 31}$ is the mass-inertia matrix, $\mathbf{C}(\mathbf{q}, \dot{\mathbf{q}}) \in \mathbb{R}^{31}$ contains the centrifugal and Coriolis forces terms, $\mathbf{G}(\mathbf{q}) \in \mathbb{R}^{31}$ is the vector of gravitational forces, $\tau \in \mathbb{R}^{31}$ is the vector of joint torques. The dynamics equations of the model were derived using the Euler–Lagrange formulation [34]. Based on [38], the Jacobian and mass-inertia matrices are used to obtain the dynamic manipulability measure as follows:

$$\mathrm{w_d} = \sqrt{\det\left[\mathbf{J}(\mathbf{q})\left(\mathbf{M}(\mathbf{q})^{\mathrm{T}}\mathbf{M}(\mathbf{q})\right)^{-1}\mathbf{J}(\mathbf{q})^{\mathrm{T}}\right]}. \tag{6}$$

This measure specifies the ability to perform end-effector accelerations in a given posture with the joint torques constrained to belong to a unit sphere. The detailed mass/inertia parameters as a fraction of total height and weight are obtained according to anthropometric tables [40].

2.3 Experimental procedure and kinematic mapping

Eleven young healthy persons (age 27.7 ± 3.3 years, mass 75.5 ± 9.0 kg, height 1.80 ± 0.06 m; $\pm$ means s.d.) without any histories of orthopedic or neurological disorders participated in the study. All the persons signed an informed consent form before starting trials. The protocol was approved by the ethical committee of the Faculty of Human Movement Sciences of VU University, Amsterdam. Subjects walked on a treadmill at three different speeds (0.56, 1.12 and 1.68 ms^{-1}), for 5 minutes in each condition. A 3D optoelectronic system (Optotrak® Northern Digital Inc., Waterloo, ON, Canada) was used for kinematic data collection of 36 reflective markers at a sampling rate of 50 Hz.

Mapping of the experimental kinematics on the model is accomplished using an inverse kinematic method. In this method, the joint angles of the model that best reproduce the experimental kinematics are obtained [12]. To find the best match between the model and experimental kinematics, an optimization problem is formulated. First, virtual markers are placed on the model that correspond to the position of the physical markers on the human subject. Then, the distances between the virtual and corresponding experimental marker positions are minimized. The cost function is expressed as

$$\min_{\mathbf{q}} \sum_{i=1}^{m} W_i \left\| x_i^{\mathrm{exp}} - x_i^{v}(\mathbf{q}) \right\|^2, \tag{7}$$

in which $\mathbf{q}$ is the vector of joint angles, x_i^{exp} is the position of experimental marker i, $x_i^{v}(\mathbf{q})$ is the position of the corresponding virtual marker i, m is the number of markers, and W_i is the weight associated with marker i. During the course of several simulations, the trial-and-error procedure was used to find weights W_i that gave results in good accordance with experiments (Table 2, Appendix B).

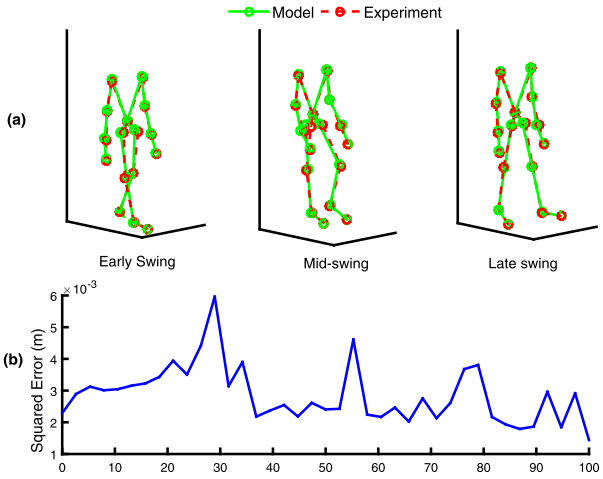

Fig. 2 (**a**) Comparison between the experimental kinematics and the simulated model; (**b**) total squared error between the position of the experimental and virtual markers

The objective function is subject to the constraints on physiological limitation of joint angles. In each frame of motion, the cost is minimized using a commercial software package (MATLAB release 2014a, The MathWorks, Inc., Natick, MA, USA) and the output which is a vector of joint angles ($\mathbf{q}$) is saved for future uses. In the current work, a hybrid genetic algorithm (HGA) which combines both deterministic and stochastic routines [8] was used to solve the optimization problem. The Crossover fraction value was 0.8 and the probability of mutation rate was not considered to be a fixed value. The adaptive feasible function of MATLAB (mutationadaptfeasible) was used as the mutation function to randomly generate directions that are adaptive with respect to the last successful or unsuccessful generation.

Statistical analyses of the current study have been done using SPM1D repeated measures ANOVA [28, 29]. This method can identify regionally specific effects.

3 Results and discussions

Figure 2(a) presents the kinematics of human and the simulation model for three selected postures of walking. The total squared error between the positions of the virtual and real markers is also depicted in Fig. 2(b). As can be seen, there is a good correspondence between the kinematics of the subject and the model obtained by the optimization.

3.1 Sensitivity analysis

The manipulability index is defined based on the Jacobian and is related to the joint variables of the model/subject. A sensitivity analysis is conducted to investigate how the variation in the manipulability of the model can be attributed to variations of joint angles. The elementary effects (EEs) method [31] was used for the sensitivity analysis to identify influential joint variables. The average of Elementary Effects of the variation of joint angles on the manipulability against their standard deviations are depicted in Figs. 3 and 4 for the swing foot and CoM, respectively.

From Fig. 3 it is apparent that the manipulability of the swing foot is more sensitive to the support hip extension/flexion, spine joint bending and swing hip extension/flexion.

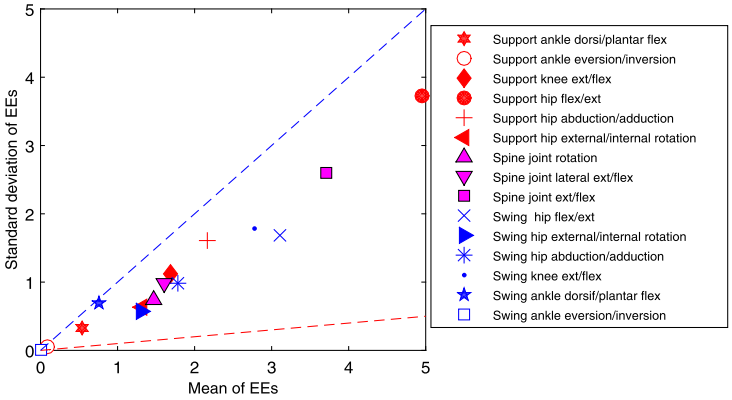

Fig. 3 Mean of Elementary Effects (EEs) and standard deviation for swing foot. Two straight lines of slopes $\sigma/\mu^* = 0.1$ and 1 define linear and monotonic (or almost monotonic) zones, respectively. The legend is abbreviated. Flex stands for the flexion and ext stands for the extension

Fig. 4 Mean of Elementary Effects (EEs) and standard deviation for CoM. Two straight lines of slopes $\sigma/\mu^* = 0.1$ and 1 define linear and monotonic (or almost monotonic) zones, respectively. The legend is abbreviated. Flex stands for flexion and ext stands for extension

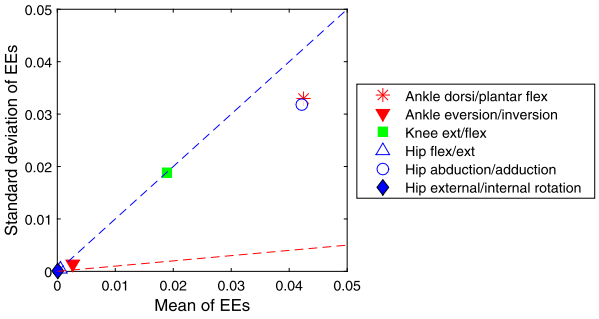

The top three sensitive parameters for the CoM manipulability index are ankle dosiflexion/plantarflexion, hip abduction/adduction and knee flexion/extension, respectively (Fig. 4).

Based on the elementary effects (EEs) method, the ratio σ/μ^* (Standard deviation/Mean) is an indicator of linearity and nonlinearity. The model response is almost linear if the ratio is smaller than 0.1. If the ratio is greater than 0.1 and smaller than 1, the model response can be considered as monotonic or almost monotonic. If the ratio is higher than 1, there are nonlinear effects or interactions. So, by plotting two straight lines of slopes $\sigma/\mu^* = 0.1$ and 1, respectively, we can graphically identify in the elementary effects scatter plot, those factors which are almost linear (below the line $\sigma/\mu^* = 0.1$) and monotonic/almost monotonic (below the line $\sigma/\mu^* = 1$). Results of Figs. 3 and 4 show that there are no nonlinear or interaction effects of the factors.

3.2 Manipulability of walking

Evaluation of the manipulability index of the swing foot during walking is presented in this section. It should be mentioned that the same results are found for both right and left swing feet. For directional analysis of the capacity to perform velocities at the swing limbs, the manipulability ellipsoids are plotted. It should be remembered that these velocity ellipsoids define the set of swing foot and hands velocities that can be obtained given a set of joint

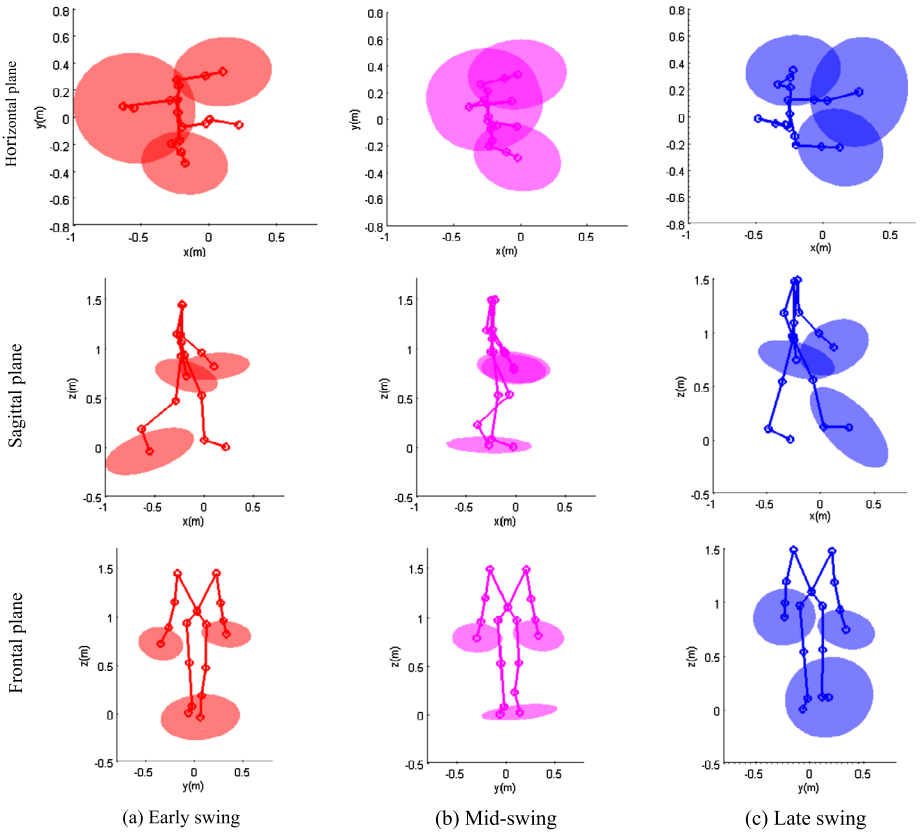

Fig. 5 Horizontal, sagittal and frontal plane views of manipulability ellipsoids at (**a**) early swing, (**b**) mid-swing, and (**c**) late swing phases of walking

Fig. 6 Three-dimensional kinematic manipulability ellipsoids for the swing foot and hands

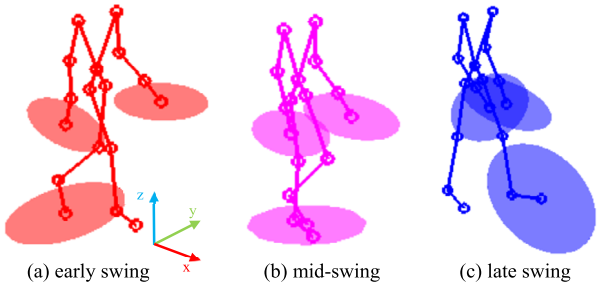

velocities of unit norm. The two-dimensional ellipsoids are shown in all three anatomical planes in Fig. 5, and the three-dimensional ellipsoids of swing limbs at three different stages of the swing phase are depicted in Fig. 6. As can be seen, there are differences between the direction and length of the principal axes of the ellipsoids. For example, during the late swing phase (Fig. 6(c)) the direction of the major axis is totally different from that during early swing phase, and also in the latter phase it is rounder than the former phase. The direction of the largest principal axis of the kinematic manipulability ellipsoid of the swing foot in

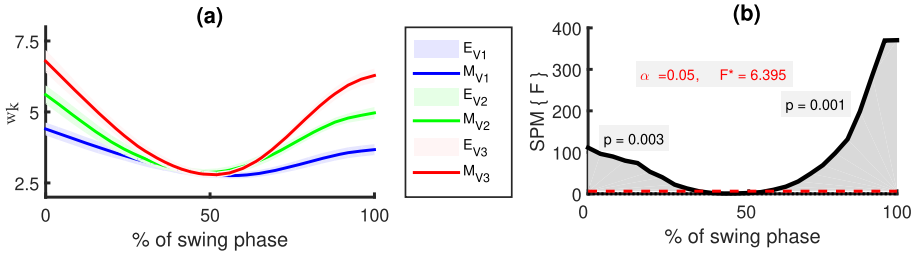

Fig. 7 (**a**) Kinematic manipulability of the swing foot for different speeds ($V1 = 0.56$ ms^{-1}, $V2 = 1.12$ ms^{-1}, and $V3 = 1.68$ ms^{-1}). Solid lines show the mean (M), and shaded clouds (E) indicate the standard deviation envelope. (**b**) SPM1D repeated measures ANOVA of swing foot for kinematic manipulability index. Three speeds were considered. Small p-value ($p \leq 0.05$) indicates that a significant difference does exist. F* is the significance level of SPM (at $\alpha = 0.05$)

the horizontal plane rotates from anterior–posterior to anteromedial–posterolateral when the subject moves from early swing phase to late swing phase (see Fig. 5). The directions of the principal axes for the hands and the swing foot are not the same during the late swing phase. In the sagittal plane, the largest axis of the swing foot ellipse rotates from anterior–superior/posterior–inferior to the anterior–inferior/posterior–superior direction. In this plane and at the mid-swing phase, the size of ellipse is smaller than the early and late swing phases. There is not a considerable change of axis direction in the frontal plane, but the variation of the volume of the manipulability ellipse is substantial.

Figure 7(a) shows the evolution of the kinematic manipulability index of the swing foot during walking. The effect of walking speed was tested using SPM1D for kinematic manipulability index of swing phase (Fig. 7(b)). With the higher speeds of walking, the kinematic manipulability of swing foot significantly increases in early and late swing phases (Fig. 7(b)). It is seen that during mid-swing phase of walking, the kinematic manipulability value is lower than that of the early and late swing phases. This result indicates a greater range of possible motions at the early and the late swing phases of walking.

Evaluation of the dynamic manipulability index of the swing foot at different speeds is presented in Fig. 8(a). As can be seen, it starts with a relatively small value during early swing phase and then it rises to maximum values during the end of the late swing phase. Unlike the kinematic manipulability index, the dynamic manipulability decreased with increasing walking speed. The effect of walking speed was tested using SPM1D for dynamic manipulability index of swing phase (Fig. 8(b)). With the higher speeds of walking, the dynamic manipulability of swing foot significantly decreases during 20% and 40% of swing phases. It should be mentioned that the consideration of unit norm torques/velocities as inputs to calculate the dynamic/kinematic manipulability does not impose any limitation to the method of the current work and the obtained results are general.

3.3 Manipulability and stability

To assess possible correlations between the manipulability and stability of walking, local and orbital dynamic stability of walking were calculated. Maximum Floquet multipliers (MaxFMs) and maximum Lyapunov exponents (λ_s) were calculated to quantify orbital stability and local stability of walking, respectively [4]. It should be mentioned that

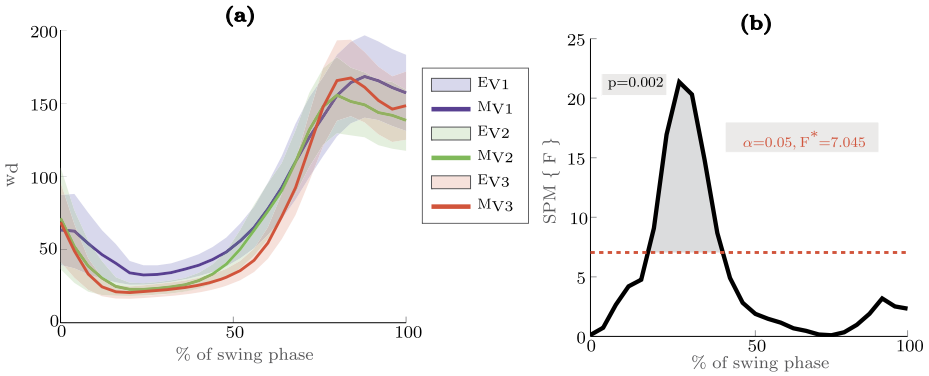

Fig. 8 (**a**) Dynamic Manipulability of swing foot for different speeds ($V1 = 0.56$ ms^{-1}, $V2 = 1.12$ ms^{-1}, and $V3 = 1.68$ ms^{-1}). Solid lines show the mean (M), and shaded clouds (E) indicate the standard deviation envelope. (**b**) SPM1D repeated measures ANOVA of swing foot for dynamic manipulability index. Three speeds were considered. Small p-value ($p \leq 0.05$) indicates that a significant difference does exist. F* is the significance level of SPM (at $\alpha = 0.05$)

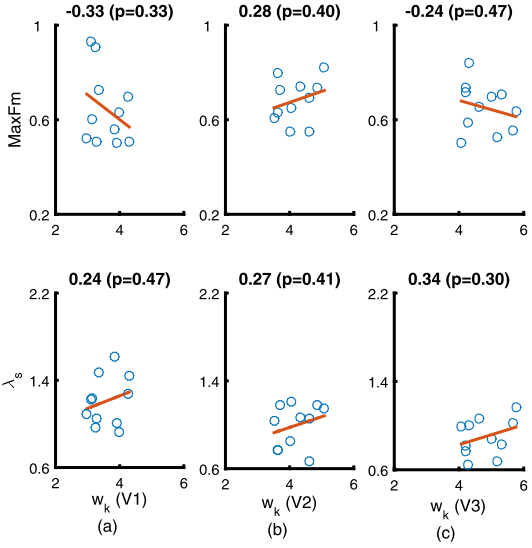

Fig. 9 Correlation between the average kinematic manipulability of swing foot and local and orbital dynamic stability measures for eleven subjects walking at (**a**) $V1 = 0.56$ ms^{-1}, (**b**) $V2 = 1.12$ ms^{-1}, and (**c**) $V3 = 1.68$ ms^{-1}. Correlation coefficients are depicted on the top of the subplots. Each p-value is the probability of getting a correlation as large as the observed value by random chance. If p is less than 0.05, then the correlation is significant

both of these measures have an inverse relation with stability. Figure 9 shows the correlations between the average kinematic manipulability of the swing phase and the stability measures of all the subjects walking at three different speeds. As seen, there are negative correlation between the manipulability and maximum Floquet multipliers at the speeds $V1$ and $V3$. For stability of a gait cycle, Floquet multipliers should remain inside the unit circle ($FM < 1$). Higher values of MaxFMs indicate a more unstable gait pattern. On the other hand, the negative correlation between the kinematic manipulability of swing foot and MaxFMs shows the importance of the manipulability for orbital dynamic stability of gait.

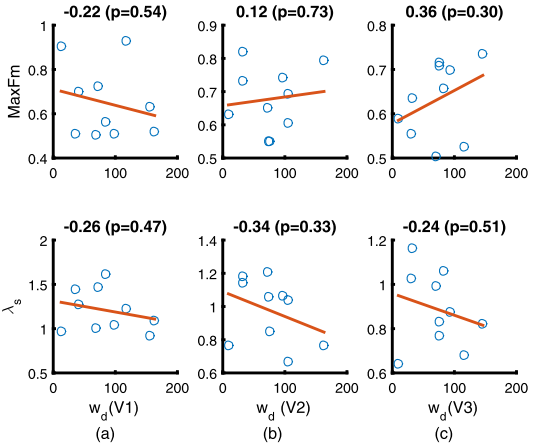

Fig. 10 Correlation between the average dynamic manipulability of swing foot and local and orbital dynamic stability measures for eleven subjects walking at (**a**) $V1 = 0.56$ ms^{-1}, (**b**) $V2 = 1.12$ ms^{-1}, and (**c**) $V3 = 1.68$ ms^{-1}. Correlation coefficients are depicted on the top of the subplots. If p is less than 0.05, then the correlation is significant

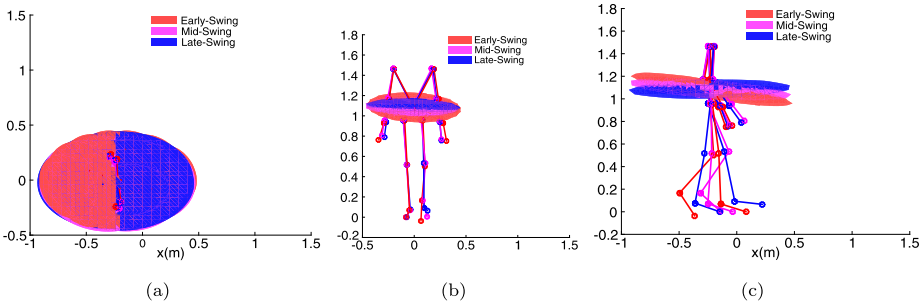

Fig. 11 The CoM manipulability ellipsoids at early, mid- and late swing phases of walking: (**a**) horizontal view, (**b**) frontal view, (**c**) sagittal view

There is a weak correlation between the kinematic manipulability of the swing foot and the local stability (Fig. 9). There are positive correlations between the kinematic manipulability and local stability measure (λ_s) at all the speeds. The correlation between the local stability measure and the kinematic manipulability of slow walking is weaker than for the others. This implies that increases in the kinematic manipulability of swing foot during higher walking speeds lead to decreased local stability, and vice versa. The correlation between the dynamic manipulability and stability was also weak (Fig. 10).

Figure 11 shows the kinematic manipulability ellipsoids of CoM at early, mid- and late swing phases. Figure 12 shows the correlation between the kinematic manipulability of CoM and the stability measures. The evolution of the kinematic manipulability of the CoM during swing phase is depicted in Fig. 13(a). The results showed no significant correlation between the kinematic manipulability of the CoM and stability of walking (Fig. 12). Although the variation of the kinematic manipulability of CoM is not significant, it is interesting that it decreases with increasing walking speed during early and mid- swing phases but not during late swing phase (Fig. 13(a)). The effect of walking speed was tested using SPM1D for CoM kinematic manipulability index of swing phase (Fig. 13(b)). With the higher speeds

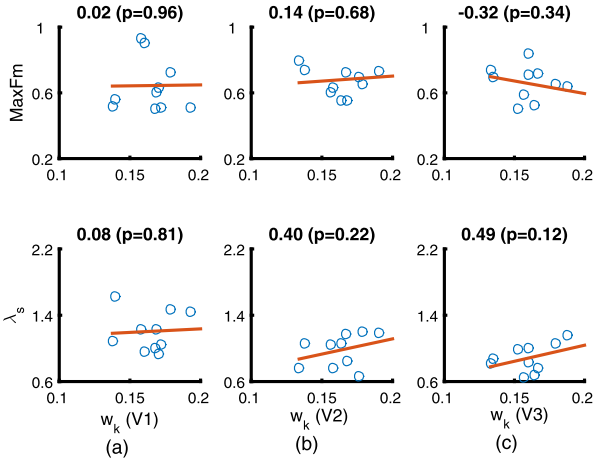

Fig. 12 Correlation between the average kinematic manipulability of CoM and local and orbital dynamic stability measures for eleven subjects walking at (**a**) $V1 = 0.56$ ms^{-1}, (b) $V2 = 1.12$ ms^{-1}, and (**c**) $V3 = 1.68$ ms^{-1}. Correlation coefficients are depicted on the top of the subplots. If p is less than 0.05, then the correlation is significant

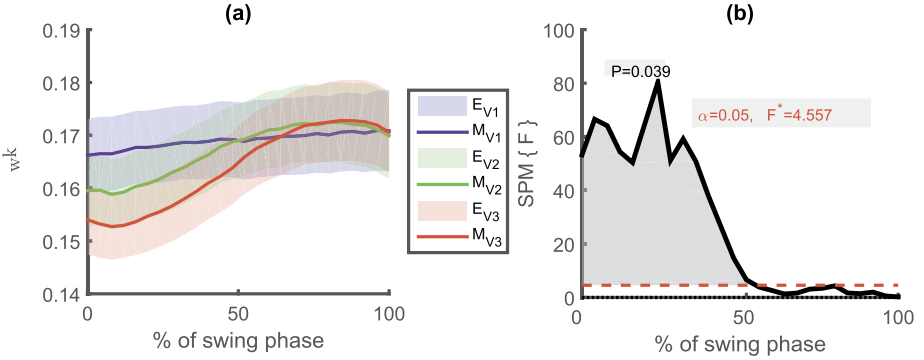

Fig. 13 (**a**) Kinematic manipulability of CoM during swing phase for different speeds ($V1 = 0.56$ ms^{-1}, $V2 = 1.12$ ms^{-1}, and $V3 = 1.68$ ms^{-1}). Solid lines show the mean (M), and shaded clouds (E) indicate the standard deviation envelope. (**b**) SPM1D repeated measures ANOVA of CoM for kinematic manipulability index. Three speeds were considered

of walking, the kinematic manipulability of CoM significantly decreases during early swing phase.

During the swing phase, the manipulability of the CoM is only related to the joint angles of the stance leg (approximating the position of the CoM in the position of the spine), whereas the manipulability of the swing foot is related to the joints of the support leg, spine and swing leg. So the degree of redundancy for the swing foot is more than that of the CoM. Nevertheless, it is clear that even a small redirection of the CoM can influence the kinematics of the swing foot and consequently its manipulability. Previous studies have indicated the importance of manipulating the CoM in foot placement [3, 11]. Our study shows that during the swing phase of normal walking the manipulability of CoM has no substantial variations.

However, the current study has some limitations, including the approximation of the CoM at the position of the spine joint. To obtain more realistic results, the real whole-body CoM should be considered.

In the current work, it has implicitly been assumed that the maximum angular velocities and driving torques of all joints are the same and the manipulability ellipsoids are obtained based on this assumption. Unit velocities and torques have been used to obtain manipulability ellipsoids. This is the other limitation of the current work. In order to obtain more realistic results, normalization of the variables should be performed and the manipulability ellipsoids should be obtained using the normalized Jacobian [43].

At last but not least, although the results of current study showed that there are no significant correlations between the manipulability and two stability measures (MaxFMs and (λ_s)), these results do not imply that there is no significant relation between the manipulability and other stability measures (for example, foot placement based stability measures). Foot placement based stability measures have recently been of interest but they do not share the same breadth of development as other methods with years of development behind them. More research is needed in this area.

4 Conclusions

In this paper, an evaluation of the manipulability of the swing phase of human walking was presented. The variation of the manipulability of the swing foot was substantial during the swing phase. The kinematic manipulability measure starts with a relatively greater value during early swing phase and then it reaches a minimum value during mid-swing phase. Eventually, it rises again to near the initial value during the end of the late swing phase. The direction of the largest principal axis of the kinematic manipulability ellipses changes over the swing phase. The dynamic manipulability of the late swing phase is higher than that of the early and mid-swing phases. The kinematic manipulability of the swing foot increased significantly with increasing walking speed during the early and late swing phases but not during mid-swing phase, whereas the dynamic manipulability decreases with increasing walking speed during entire the swing phase. The sensitivity analysis showed that the manipulability of swing foot is most sensitive to the contralateral hip flexors/extensors.

The relation between stability and manipulability of the swing foot was also investigated in this study. The results indicate a weak relation between the manipulability of the swing foot and local and orbital stability of walking. The analysis indicated that the kinematic manipulability of the CoM has no significant changes during the swing phase of walking. There was no significant relation between the kinematic manipulability of the CoM and stability during the swing phase of walking.

The results of this study encourage further research elucidating the role of manipulability in prediction of foot placement that can directly affect the maneuverability and disturbance rejection of humans or humanoid robots. It may also be possible to use the manipulability index in prediction of singularity and configurations locks in path planning of biped robots. This index may also be used as a criterion in rehabilitation to assess the improvement of performance.

Acknowledgements S. M Bruijn was funded by a VIDI grant (016.Vidi.178.014) from the Dutch Organization for Scientific Research (NWO).

Appendix A: DH table of the model

DH parameters of the body model based on the coordinates depicted in Fig. 1 are as follows:

Table 1 DH parameters of the model of current study

DoF	a_i	α_i	d_i	q_i	Branch/segment
1	r_{foot}	0	0	q_1	Right leg
2	0	$\pi/2$	0	q_2	
3	r_{calf}	$-\pi/2$	0	q_3	
4	r_{thigh}	0	0	q_4	
5	0	$\pi/2$	0	q_5	
6	0	$\pi/2$	0	q_6	
7	a_1	0	d_1	q_7	Spine
8	0	$\pi/2$	0	q_8	
9	0	$-\pi/2$	0	q_9	
10	a_2	0	d_2	q_{10}	Right arm
11	0	$-\pi/2$	0	q_{11}	
12	0	$-\pi/2$	0	q_{12}	
13	r_{arm}	$\pi/2$	0	q_{13}	
14	0	$\pi/2$	0	q_{14}	
15	0	$-\pi/2$	$r_{forearm}$	q_{15}	
16	0	$\pi/2$	0	q_{16}	
17	r_{hand}	0	0	q_{17}	
18	$-d_1$	0	$-a_1$	$q_{18} = q_{10}$	Left leg
19	0	$-\pi/2$	0	q_{19}	
20	0	$\pi/2$	0	q_{20}	
21	l_{thigh}	$\pi/2$	0	q_{21}	
22	l_{calf}	0	0	q_{22}	
23	0	$\pi/2$	0	q_{23}	
24	0	$-\pi/2$	l_{foot}	q_{24}	
25	a_2	0	$-d_2$	$q_{25} = q_{10}$	Left arm
26	0	$-\pi/2$	0	q_{26}	
27	0	$-\pi/2$	0	q_{27}	
28	l_{arm}	$\pi/2$	0	q_{28}	
29	0	$-\pi/2$	0	q_{29}	
30	0	$-\pi/2$	$l_{forearm}$	q_{30}	
31	0	$\pi/2$	0	q_{31}	
32	0	0	l_{hand}	q_{32}	

The transformation matrix is equal to

$$ {}^{j-1}T_j = \begin{bmatrix} c_{\theta_j} & -s_{\theta_j} c_{\alpha_j} & s_{\theta_j} s_{\alpha_j} & a_j c_{\theta_j} \\ s_{\theta_j} & c_{\theta_j} c_{\alpha_j} & -c_{\theta_j} s_{\alpha_j} & a_j s_{\theta_j} \\ 0 & s_{\alpha_j} & c_{\alpha_j} & d_j \\ 0 & 0 & 0 & 1 \end{bmatrix}, $$

in which $j = 1, 2, \ldots, n$.

Appendix B: Weights of the cost function (7)

The weights (W_i) that have been used in the cost function of the inverse kinematics problem (7) is summarized in the following table:

Table 2 W_i of the cost function

Marker name	Weight	Marker name	Weight	Marker name	Weight
Right toe	1	Right ankle	10	Right knee	10
Left toe	1	Left ankle	10	Left knee	10
Right hip	10	Right wrist	5	Right shoulder	10
Left hip	10	Left wrist	5	Left shoulder	10
Right elbow	20	Right hand	30	pelvis	10
Left elbow	20	Left hand	30		

References

1. Acasio, J., Fey, N.P., Gordon, K.E., et al.: Stability-maneuverability trade-offs during lateral steps. Gait Posture **52**, 171–177 (2017)
2. Baetz, G., Scheint, M., Wollherr, D.: Toward dynamic manipulation for humanoid robots: experiments and design aspects. Int. J. Humanoid Robot. **8**(03), 513–532 (2011)
3. Bauby, C.E., Kuo, A.D.: Active control of lateral balance in human walking. J. Biomech. **33**(11), 1433–1440 (2000)
4. Bruijn, S., Meijer, O., Beek, P., Van Dieën, J.: Assessing the stability of human locomotion: a review of current measures. J. R. Soc. Interface **10**(83), 20120999 (2013)
5. Chiaacchio, P., Concilio, M.: The dynamic manipulability ellipsoid for redundant manipulators. In: Proceedings. 1998 IEEE International Conference on Robotics and Automation, vol. 1, pp. 95–100. IEEE Press, New York (1998)
6. Cotton, S., Fraisse, P., Murray, A.P.: On the manipulability of the center of mass of humanoid robots: application to design. In: ASME 2010 International Design Engineering Technical Conferences and Computers and Information in Engineering Conference, pp. 1259–1267 (2010). American Society of Mechanical Engineers
7. Endo, H.: Application of robotic manipulability indices to evaluate thumb performance during smartphone touch operations. Ergonomics **58**(5), 736–747 (2015)
8. Gen, M., Zhang, W., Lin, L., Yun, Y.: Recent advances in hybrid evolutionary algorithms for multiobjective manufacturing scheduling. Comput. Ind. Eng. **112**, 616–633 (2017)
9. Gravagne, I.A., Walker, I.D.: Manipulability, force, and compliance analysis for planar continuum manipulators. IEEE Trans. Robot. Autom. **18**(3), 263–273 (2002)

10. Gu, Y., Lee, C.G., Yao, B.: Feasible center of mass dynamic manipulability of humanoid robots. In: 2015 IEEE International Conference on Robotics and Automation, ICRA, pp. 5082–5087. IEEE Press, New York (2015)
11. Hof, A.L., van Bockel, R.M., Schoppen, T., Postema, K.: Control of lateral balance in walking: experimental findings in normal subjects and above-knee amputees. Gait Posture **25**(2), 250–258 (2007)
12. Huang, Q., Yu, Z., Zhang, W., Xu, W., Chen, X.: Design and similarity evaluation on humanoid motion based on human motion capture. Robotica **28**(5), 737–745 (2010)
13. Inoue, K., Yoshida, H., Arai, T., Mae, Y.: Mobile manipulation of humanoids-real-time control based on manipulability and stability. In: IEEE International Conference on Robotics and Automation, 2000. Proceedings, ICRA'00, vol. 3, pp. 2217–2222. IEEE Press, New York (2000)
14. Jacquier-Bret, J., Gorce, P., Rezzoug, N.: The manipulability: a new index for quantifying movement capacities of upper extremity. Ergonomics **55**(1), 69–77 (2012)
15. Jacquier-Bret, J., Rezzoug, N., Gorce, P.: Effect of spinal cord injury at c6–c7 on global upper-limb coordination during grasping: manipulability approach. IRBM **34**(1), 69–73 (2013)
16. Klein, C.A., Blaho, B.E.: Dexterity measures for the design and control of kinematically redundant manipulators. Int. J. Robot. Res. **6**(2), 72–83 (1987)
17. Kobayashi, Y., Minami, M., Yanou, A., Maeba, T.: Dynamic reconfiguration manipulability analyses of humanoid bipedal walking. In: 2013 IEEE International Conference on Robotics and Automation, ICRA, pp. 4779–4784. IEEE Press, New York (2013)
18. Lee, I., Oh, J.H.: Humanoid posture selection for reaching motion and a cooperative balancing controller. J. Intell. Robot. Syst. **81**(3–4), 301–316 (2016)
19. Lenarčič, J., Klopčar, N.: Positional kinematics of humanoid arms. Robotica **24**(1), 105–112 (2006)
20. Maneewarn, T., Boonprakob, A.: Walking pattern modification using manipulability ellipsoid for biped robot. In: IEEE International Conference on Robotics and Biomimetics, 2008, ROBIO 2008, pp. 160–165. IEEE Press, New York (2009).
21. Minami, M., Takahara, M.: Avoidance manipulability for redundant manipulators. In: Proceedings. 2003 IEEE/ASME International Conference on Advanced Intelligent Mechatronics, AIM 2003, vol. 1, pp. 314–319. IEEE Press, New York (2003)
22. Minami, M., Zhang, T., Yu, F., Nakamura, Y., Yasukura, O., Song, W., Yanou, A., Deng, M.: Reconfiguration manipulability analyses for redundant robots in view of structure and shape. In: SCIS & ISIS, SCIS & ISIS 2010, pp. 971–976 (2010). Japan Society for Fuzzy Theory and Intelligent Informatics
23. Müller, A.: Manipulability and static stability of parallel manipulators. Multibody Syst. Dyn. **9**(1), 1–23 (2003)
24. Nagatani, K., Hirayama, T., Gofuku, A., Tanaka, Y.: Motion planning for mobile manipulator with keeping manipulability. In: IEEE/RSJ International Conference on Intelligent Robots and Systems, 2002, vol. 2, pp. 1663–1668. IEEE Press, New York (2002)
25. Naksuk, N., Lee, C.G.: Zero moment point manipulability ellipsoid. In: Proceedings 2006 IEEE International Conference on Robotics and Automation, ICRA 2006, pp. 1970–1975. IEEE Press, New York (2006)
26. Ota, Y., Yoneda, K., Muramatsu, Y., Hirose, S.: Development of walking and task performing robot with bipedal configuration. In: Proceedings. 2001 IEEE/RSJ International Conference on Intelligent Robots and Systems, vol. 1, pp. 247–252. IEEE Press, New York (2001)
27. Padois, V., Ivaldi, S., Babič, J., Mistry, M., Peters, J., Nori, F.: Whole-body multi-contact motion in humans and humanoids: advances of the CoDyCo European project. Robot. Auton. Syst. **90**, 97–117 (2017)
28. Pataky, T.C.: Generalized *n*-dimensional biomechanical field analysis using statistical parametric mapping. J. Biomech. **43**(10), 1976–1982 (2010)
29. Pataky, T.C., Vanrenterghem, J., Robinson, M.A.: Zero- vs. one-dimensional, parametric vs. non-parametric, and confidence interval vs. hypothesis testing procedures in one-dimensional biomechanical trajectory analysis. J. Biomech. **48**(7), 1277–1285 (2015)
30. Perry, J.A., Srinivasan, M.: Walking with wider steps changes foot placement control, increases kinematic variability and does not improve linear stability. R. Soc. Open Sci. **4**(9), 160627 (2017)
31. Pianosi, F., Sarrazin, F., Wagener, T.: A Matlab toolbox for global sensitivity analysis. Environ. Model. Softw. **70**, 80–85 (2015)
32. Samy, V., Kheddar, A.: Falls control using posture reshaping and active compliance. In: 2015 IEEE-RAS 15th International Conference on Humanoid Robots (Humanoids), pp. 908–913. IEEE Press, New York (2015)
33. Shen, K., Li, X., Tian, H., Matsuno, T., Minami, M.: Analyses of biped walking posture by dynamical-evaluating index. Artif. Life Robot., 1–10 (2017)
34. Spong, M.W., Hutchinson, S., Vidyasagar, M., et al.: Robot Modeling and Control, vol. 3. Wiley, New York (2006)

35. Tagawa, Y., Yamashita, T.: Controllability of body motion in bipedal locomotion. In: Proceedings. IEEE/RSJ International Workshop on Intelligent Robots and Systems' 89. The Autonomous Mobile Robots and Its Applications, IROS'89, pp. 180–186. IEEE Press, New York (1989)
36. Tripp, B.P., McIlroy, W.E., Maki, B.E.: Online mutability of step direction during rapid stepping reactions evoked by postural perturbation. IEEE Trans. Neural Syst. Rehabil. Eng. **12**(1), 140–152 (2004)
37. Vahrenkamp, N., Asfour, T., Metta, G., Sandini, G., Dillmann, R.: Manipulability analysis. In: 2012 12th IEEE-RAS International Conference on Humanoid Robots (Humanoids), pp. 568–573. IEEE Press, New York (2012)
38. Yoshikawa, T.: Dynamic manipulability of robot manipulators. Trans. Soc. Instrum. Control Eng. **21**(9), 970–975 (1985)
39. Wang, Y., Srinivasan, M.: Stepping in the direction of the fall: the next foot placement can be predicted from current upper body state in steady-state walking. Biol. Lett. **10**(9), 20140405 (2014)
40. Winter, D.A.: Biomechanics and Motor Control of Human Movement. Wiley, New York (2009)
41. Xiao, T., Li, M., Huang, Q., Zhang, W., He, L.: Analysis of pushing manipulation by humanoid robot BHR-2 during dynamic walking. In: 2007 IEEE International Conference on Automation and Logistics, pp. 3000–3005. IEEE Press, New York (2007)
42. Yoshikawa, T.: Manipulability of robotic mechanisms. Int. J. Robot. Res. **4**(2), 3–9 (1985)
43. Yoshikawa, T.: Foundations of Robotics: Analysis and Control. MIT Press, Cambridge (1990)